

# The relation between broad lines and $\gamma$ -ray luminosities in *Fermi* blazars

T. Sbarrato<sup>1\*</sup>, G. Ghisellini<sup>2</sup>, L. Maraschi<sup>3</sup>, M. Colpi<sup>1</sup>.

<sup>1</sup>*Department of Physics G. Occhialini, University of Milano-Bicocca, Piazza della Scienza 3, 20126 Milano, Italy*

<sup>2</sup>*INAF – Osservatorio Astronomico di Brera, Via Bianchi 46, I-23807 Merate, Italy*

<sup>3</sup>*INAF – Osservatorio Astronomico di Brera, Via Brera 28, I-20100 Milano, Italy*

18 May 2012

## ABSTRACT

We study the relation between the mass accretion rate, the jet power, and the black hole mass of blazars. To this aim, we make use of the Sloan Digital Sky Survey (SDSS) and the 11 months catalog of blazars detected at energies larger than 100 MeV by the Large Area Telescope (LAT) onboard the *Fermi* satellite. This allows to construct a relatively large sample of blazars with information about the luminosity (or upper limits) of their emission lines used as a proxy for the strength of the disc luminosity and on the luminosity of the high energy emission, used as a proxy for the jet power. We find a good correlation between the luminosity of the broad lines and the  $\gamma$ -ray luminosity as detected by *Fermi*, both using absolute values of the luminosities and normalising them to the Eddington value. The data we have analyzed confirm that the division of blazars into BL Lacs and Flat Spectrum Radio Quasars (FSRQs) is controlled by the line luminosity in Eddington units. For small values of this ratio the object is a BL Lac, while it is a FSRQs for large values. The transition appears smooth, but a much larger number of objects is needed to confirm this point.

**Key words:** BL Lacertae objects: general — quasars: general — radiation mechanisms: non-thermal — gamma-rays: theory — X-rays: general

## 1 INTRODUCTION

The classic division between Flat Spectrum Radio Quasars (FSRQs) and BL Lac objects is mainly based on the Equivalent Width (EW) of the emission lines. Objects with rest frame  $EW > 5 \text{ \AA}$  are classified as FSRQs (see e.g. Urry & Padovani 1995). Marcha et al. (1996) and Landt, Padovani & Giommi (2002) discussed the Ca H&K 4000- $\text{\AA}$  (rest frame) break as a criterion helping to distinguish BL Lac objects from low-luminosity radio galaxies. Furthermore, Marcha et al. (1996) proposed that objects with a weak Ca break and with EW even larger than  $5 \text{ \AA}$  should be classified as BL Lacs. On the other hand, Scarpa & Falomo (1997) showed a continuity between BL Lac and FSRQs concerning the luminosity of the Mg II line, taken as an indication against a clear separation of blazars in the two subclasses. Landt et al. (2004), instead, considered *narrow* lines, such as [O II] and [O III], and found that it is possible to separate *intrinsically* weak and strong line blazars in the [O II] and [O III] equivalent width plane.

The classification scheme based on the EW of the broad lines has been adopted both because it is observationally simple, and because it was thought to measure the relative importance of the non-thermal jet emission over the thermal one. However, we now

know that the jet electromagnetic output is often dominated by the emission at higher energies (hard X-rays and  $\gamma$ -rays), and therefore the EW of the optical emission lines is not a good measure of the jet dominance. Furthermore, the jet flux is much more variable than the underlying thermal emission, causing the measured EW to vary. Occasionally, a blazar with very luminous emission lines, that should be classified as a FSRQ, can instead appear as BL Lacs when the optical jet flux is particularly strong. Conversely, a BL Lac in a particular faint state could show broad emission lines that, albeit weak, can have EW greater than  $5 \text{ \AA}$ . In Ghisellini et al. (2011; G11 thereafter) we have therefore proposed a more physical distinction between the two classes of blazars, based on the luminosity of the broad emission lines measured in Eddington units:  $L_{\text{BLR}}/L_{\text{Edd}}$ . We proposed that when  $L_{\text{BLR}}/L_{\text{Edd}} \gtrsim 5 \times 10^{-4}$  the objects are FSRQs, and are BL Lacs below this value. Normalizing to the Eddington luminosity ensures the appropriate comparison among objects of different black hole masses.

The sample of blazars studied in G11 was limited, since it was based on a small sub-sample of bright FSRQs detected in  $\gamma$ -rays by the *Fermi* satellite during the first 3 months of operation (LBAS sample, Abdo et al. 2009), and on BL Lac objects detected by *Fermi* during the first 11 months (1LAC sample, Abdo et al. 2010a), with a relatively steep  $\gamma$ -ray energy spectral index  $\alpha_\gamma$  ( $\alpha_\gamma > 1.2$ ). These BL Lacs occupy the region of the spectral index –  $\gamma$ -ray lumi-

\* Email: tullia.sbarrato@brera.inaf.it

osity ( $\alpha_\gamma$ – $L_\gamma$ ) plane occupied mainly by FSRQs (see Ghisellini, Maraschi & Tavecchio 2009).

Since the broad emission lines are produced by clouds photo-ionized by the radiation produced by the accretion disc, there is a direct relation between  $L_{\text{BLR}}$  and the accretion disc luminosity  $L_d$ . Therefore, measuring the broad line luminosities, we have information on the disc luminosity even when it is not directly visible, as often occurs in blazars whose optical continuum is dominated by the jet flux. In turn, by knowing  $L_{\text{BLR}}$  and the bolometric jet luminosity, we can then study the relation between the jet and the accretion power. This in fact is the final aim of these studies. Earlier attempts to find the ratio between the jet and the accretion power were done by e.g. Celotti, Padovani & Ghisellini (1997) and by D’Elia, Padovani & Landt (2003): the novelty here is on one hand the way to estimate the jet power, and on the other hand the large number of sources for which the  $\gamma$ -ray detection ensures a good estimate of the jet power (or at least a good proxy for it), coupled with the large number of blazars present in the Sloan Digital Sky Survey (SDSS; York et al. 2000) with spectroscopic data.

Another important ingredient for this line of research is the black hole mass, allowing to measure luminosities and powers in Eddington units. Besides allowing to compare objects with different black hole masses, it allows to investigate if the accretion regime has indeed a transition, from radiatively efficient to inefficient, when the mass accretion rate in Eddington units  $\dot{M}/\dot{M}_{\text{Edd}}$  goes below a critical value (see e.g. Narayan, Garcia & McClintock 1997), and to see how this influences the jet power. For instance, the division between BL Lacs and FSRQs in the sample of blazars detected during the first three months of the *Fermi* all sky survey (LBAS) seems to corresponds to disc luminosities  $L_d/L_{\text{Edd}} \sim 10^{-2}$  (Ghisellini, Maraschi & Tavecchio 2009; see also the earlier proposal about the division of FR I and FR II radio-galaxies in Ghisellini & Celotti 2001).

For these reasons we are motivated to enlarge the original sample of G11, studying all blazars for which we can have information about their emission lines (as a proxy for the disc luminosity), their  $\gamma$ -ray luminosity (as a proxy for the jet power), and their black hole mass. The two largest samples useful for this study are the SDSS and the *Fermi* 1LAC sample. In §2 we present the samples used for this work and in §3 we discuss how we have derived the broad line luminosities, or their upper limits. In §4 we present the relation between  $L_{\text{BLR}}$  and the  $\gamma$ -ray luminosities, and we discuss our findings in §5.

## 2 THE SAMPLES

We are interested in grouping a large number of blazars with reliable measures of Broad Line Region and  $\gamma$ -ray luminosities. The Sloan Digital Sky Survey (SDSS), that provides the largest publicly available catalog of spectral objects, and the Large Area Telescope (LAT) onboard the *Fermi Gamma-Ray Space Telescope* constitute optimal devices to investigate in this direction.

We tried to select for our analysis the largest group of blazars with reliable redshift and black hole mass measures. At first, we grouped a sample of optically selected quasars from the SDSS (seventh data release, DR7), that have been deeply analysed by Shen et al. (2011; hereafter S11) and are *Fermi*-detected. Furthermore, in order to enlarge our analysis towards lower luminosities, we included in our study an optically selected group of BL Lac candidates. The BL Lacs that we took in consideration are supposed to be lineless, but their redshift and black hole masses have been de-

rived in the work by Plotkin et al. (2011; hereafter P11) from the galaxy spectral absorption features. In the end, we tried to look for possible intermediate objects, that have been excluded both from SDSS DR7 quasar catalog and P11 BL Lacs catalog. For this purpose, we selected a small group of AGNs from the previous SDSS data release (DR6, Adelman-McCarthy et al. 2008) that are *Fermi*-detected.

### 2.1 1LAC sample

This is the AGN sample resulting after 11 months of operation of the Large Area Telescope (LAT) onboard the *Fermi* satellite (First LAT AGN Catalog, 1LAC, Abdo et al. 2010a). As revised in Ackermann et al. (2011), this sample is made by 671 sources at high Galactic latitude ( $|b| > 10^\circ$ ). The statistical significance of the *Fermi* detection was required to be  $\text{TS} > 25$  (TS stands for Test Statistics, see Mattox et al. 1996 for the definition.  $\text{TS}=25$  approximately corresponds to  $5\sigma$ ).

By requiring that the associations of the detected sources have a probability  $P \geq 80\%$  and that there is only one AGN in the positional error box of the *Fermi* detection, the *Fermi* team has constructed the *clean* 1LAC sample, composed of 599 AGNs. Of these, 248 are classified by the *Fermi*/LAT team as FSRQs and 275 as BL Lacs. The remaining sources are either of unknown blazar type (50) or non-blazar AGNs (26). We then focus on the 248 FSRQs and 275 BL Lacs. All FSRQs have known redshift, while for about half of the BL Lac objects the redshift is still unknown.

### 2.2 SDSS DR7 Quasar sample

We have collected at first a group of optically selected quasars. The SDSS provides a quasar catalog out of the Data Release 7, that includes 105783 objects and has been spectrally analysed by S11. This sample includes quasars that have luminosities larger than  $M_i = -22$  [i.e.  $\nu L_\nu(5100 \text{ \AA}) = 10^{44} \text{ erg s}^{-1}$ ], that have at least one emission line with  $\text{FWHM} > 1000 \text{ km s}^{-1}$  and a reliable spectroscopical redshift. For this group of sources S11 calculated continuum and emission line measurements around the  $\text{H}\alpha$ ,  $\text{H}\beta$ ,  $\text{MgII}$  and  $\text{CIV}$  regions, and derived virial black hole masses with different calibrations, along with what they consider the best estimate. The broad line luminosities and the best estimate of the black hole masses are considered for our work.

From the cross-correlation with the 1LAC sample, we obtained a group of 49 *Fermi* detected and optically selected quasars. We excluded 3 objects because S11 do not provide a reliable black hole mass estimate. Therefore, the quasar sample under study includes 46 objects, that are listed in Table 1. Note that requiring that the objects have a broad emission line with measurable FWHM automatically excludes BL Lac objects with very weak or no emission lines.

### 2.3 Plotkin et al. (2011) BL Lac sample

We included in our analysis all the optically selected BL Lacs that are present in the work by P11. In their work, P11 start from an original sample of 723 BL Lac candidates with  $\text{EW} < 5 \text{ \AA}$ , that are included in the DR7 general catalog (for selection details, see Plotkin et al. 2010). From this original sample, they selected 143 BL Lac candidates with reliable redshift limited to  $z < 0.4$ , that match to a FIRST and/or NVSS radio source and are radio-loud (FIRST stands for Faint Images of the Radio Sky at 20 cm, White

et al. 1997; NVSS stands for NRAO VLA Sky Survey, Condon et al. 1998). Then they apply a spectral decomposition in order to separate the galaxy and AGN spectral components. Only 71 out of the 143 BL Lacs could be successfully decomposed. For this smaller sample of 71 BL Lacs, black hole masses are derived from the  $M$ – $\sigma_*$  relation.

A similar study on black hole masses of SDSS BL Lac objects has been performed in a work by León-Tavares et al. (2011). The authors started from a sample of BL Lacs included in the SDSS Data Release 5 (DR5) and radio-detected by FIRST. This original BL Lac sample was selected by Plotkin et al. (2008). León-Tavares et al. performed a spectral decomposition similar to the one in P11 on objects in the redshift range  $0.06 < z < 0.5$ . They obtain the black hole mass estimates for 78 BL Lacs, using the  $M$ – $\sigma_*$  relation. The results of León-Tavares et al. (2011) and those of P11 are very similar and the two works are consistent. We then decided to use the P11 data.

We cross-correlated the P11 sample with the clean 1LAC sample. 10 BL Lacs out of the 71 are detected by *Fermi*, hence we have measures of their  $\gamma$ -ray luminosities. For the other 61 sources, we derived an upper limit on their  $\gamma$ -ray fluxes, based on the sensitivity limit of LAT for objects with  $\Gamma_\gamma \simeq 2$ . Therefore, the upper limit in flux for these 61 BL Lacs is fixed at  $F_{ph} = 5 \times 10^{-9}$  ph cm $^{-2}$  s $^{-1}$ . The overall BL Lac sample under study includes 71 objects, that are listed in Table 2.

## 2.4 SDSS DR6 sample

We selected a last group of sources from the Data Release 6 (DR6) of the SDSS, in order to include in our analysis possible optically intermediate objects, that may have been excluded from the S11 and P11 catalogs. Therefore, we cross-correlated the SDSS DR6 and the clean 1LAC and obtained a group of 20 additional sources, not contained in the samples mentioned above. Three of these sources have no reliable redshifts, and we excluded them from our sample. Since for this group of sources we do not have a black hole mass estimate, we have chosen to assign them an average value of  $M = 5 \times 10^8 M_\odot$ . This last group of intermediate blazars includes 17 objects, that are listed in Table 3.

To sum up, the sample on which we work is composed by:

- 46 *Fermi*-detected, optically selected FSRQs from S11. These objects have detection both on  $L_{BLR}$  and  $L_\gamma$ , and have black hole masses estimated by S11.
- 10 *Fermi*-detected, optically selected BL Lacs from P11. Because of their original selection, these sources do not show any emission line. Therefore, we calculated the upper limit on  $L_{BLR}$ , while detections are available for  $L_\gamma$ . The 1LAC catalog provides for one of these sources an upper limit instead of a detection. P11 provide mass estimates for all these objects.
- 61 optically selected BL Lacs from P11 that are not *Fermi*-detected. As the other 10 sources from P11, they have mass estimates (from P11) and upper limits on  $L_{BLR}$ , but in addition we calculated upper limits on  $L_\gamma$ , too.
- 14 *Fermi*-detected objects that are included in the DR6 general sample. These objects do not show broad emission lines in their spectra, hence we calculated upper limits on their  $L_{BLR}$ . In DR6 there are no estimates of the black hole mass, hence we assigned to these objects an average mass value ( $M = 5 \times 10^8 M_\odot$ ).
- 3 *Fermi*-detected blazars that are included in the DR6 sample. These objects show at least one emission line in their spectra, hence

they have detections on both  $L_{BLR}$  and  $L_\gamma$ . For one of them, we calculated a mass estimate from the FWHM of the H $\beta$  line, while we assigned to the others an average mass value.

In total, we have 49 objects with detections on both  $L_{BLR}$  and  $L_\gamma$ , 23 with upper limits on  $L_{BLR}$  and detections on  $L_\gamma$  and 62 with upper limits on both luminosities. In the following, when discussing the relation between the BLR and the  $\gamma$ -ray luminosity, we will add to our sample other 30 blazars studied in G11, that are listed in Table 4. Of these 30 objects, 14 are FSRQs and 16 are BL Lacs (12 LBLs and 4 HBLs). 29 have measured  $L_{BLR}$  and  $\gamma$ -ray detections, while one has an upper limit on  $L_{BLR}$  and a  $\gamma$ -ray detection. The total number of blazars with measured  $L_{BLR}$ ,  $L_\gamma$  and black hole mass is therefore 78.

## 3 BROAD LINE LUMINOSITIES

We have taken the luminosity of the emission lines of the blazars in the SDSS DR7 Quasar sample directly from the listed values in the S11 catalog. For calculating the total luminosity of the broad lines, we have followed Celotti, Padovani & Ghisellini (1997). Specifically we set the Ly $\alpha$  flux contribution to 100, the relative weight of H $\alpha$ , H $\beta$ , MgII and CIV lines respectively to 77, 22, 34 and 63 (see Francis et al. 1991). The total broad line flux is fixed at 555.76. The  $L_{BLR}$  value or upper limit of each source has been derived using these proportions. In Tab. 1 we list these blazars reporting the type of lines used for calculating  $L_{BLR}$  and the values of the estimated  $L_{BLR}$  and the observed  $L_\gamma$ . When more than one line is present, we calculate the simple average of the  $L_{BLR}$  estimated from each line.

### 3.1 Upper limits on the broad line luminosity

While the SDSS DR7 Quasar sample is selected in order to contain spectra with prominent broad emission lines, that have been measured by S11, the other two samples include mostly lineless objects. In these cases, we need to derive upper limits on the line fluxes ( $UL_{F_{line}}$ ).

To this aim, the observed spectrum has been fitted with a power-law model, with the addition of possible absorption or narrow emission features modeled as Gaussian profiles. Absorption lines are well visible in the spectra included in P11 BL Lac sample and the P11 work itself provides the variance of each absorption feature ( $\sigma_*$ ). Such a modeling includes the lineless power-law and the narrow features. The broad emission line for which we want to obtain the upper limit is accounted as an additional Gaussian profile, with a variable flux value  $F_{line}$  and a FWHM fixed at the average value  $v_{FWHM} = 4000$  km s $^{-1}$ , as suggested in Decarli et al. (2011). This value is an average for all blazars, and it is consistent with the median FWHM values that can be obtained from the whole SDSS Quasar sample. Even though in the case of BL Lacs the average value is possibly slightly smaller, we prefer to maintain a larger average FWHM value, in order to derive more conservative (i.e. less stringent) upper limits. To define the  $UL_{F_{line}}$  we perform a  $\chi^2$  test, varying the  $F_{line}$  value until our model returns an unacceptable fit. Then we define the upper limit on the line flux as the  $F_{line}$  for which we obtain  $\chi^2 > \chi^2(99\%)$ . Over this critical value, the model is no more acceptable to fit the data, and we should actually see a broad line emerging over the continuum, if present. In order to derive meaningful upper limits, we required a signal-to-noise ratio  $S/N > 5$  in the wavelength interval in which we performed our analysis. Hence we checked the signal-to-noise ratios

Name	RA	DEC	$z$	$\log M/M_{\odot}$	Lines	$L_{\text{BLR}}$ [ $10^{42}$ erg/s]	$L_{\gamma}$ [ $10^{45}$ erg/s]
[1]	[2]	[3]	[4]	[5]	[6]	[7]	[8]
CGRaBS J0011+0057	00 11 30.40	+00 57 51.7	1.493	8.95	MgII	472.91	217.51
B3 0307+380	03 10 49.87	+38 14 53.8	0.816	8.23	H $\beta$ MgII	65.97	54.97
B2 0743+25	07 46 25.87	+25 49 02.1	2.978	9.59	CIV	4199.17	3849.95
OJ 535	08 24 47.24	+55 52 42.6	1.418	9.42	MgII	2004.82	643.44
B2 0827+24	08 30 52.08	+24 10 59.8	0.941	9.01	MgII	974.10	227.73
PKS 0906+01	09 09 10.09	+01 21 35.6	1.025	9.32	MgII	1883.33	462.35
0917+444	09 20 58.46	+44 41 54.0	2.188	9.25	MgII CIV	7075.62	8261.87
0917+62	09 21 36.23	+62 15 52.1	1.453	9.37	MgII	978.32	349.93
B2 0920+28	09 23 51.52	+28 15 25.1	0.744	8.80	H $\beta$ MgII	257.91	52.06
CGRaBS J0937+5008	09 37 12.32	+50 08 52.1	0.275	8.29	H $\alpha$ H $\beta$	18.18	4.59
CGRaBS J0941+2728	09 41 48.11	+27 28 38.8	1.306	8.68	MgII	4843.97	119.81
CRATES J0946+1017	09 46 35.06	+10 17 06.1	1.005	8.52	MgII	639.52	91.52
CGRaBS J0948+0022	09 48 57.31	+00 22 25.5	0.584	7.77	H $\beta$ MgII	126.83	101.32
B2 0954+25A	09 56 49.87	+25 15 16.0	0.708	9.34	H $\beta$ MgII	789.15	32.10
4C +55.17	09 57 38.18	+55 22 57.7	0.899	8.96	MgII	374.96	453.58
CRATES J1016+0513	10 16 03.13	+05 13 02.3	1.713	9.11	MgII CIV	463.36	2002.10
B3 1030+415	10 33 03.70	+41 16 06.2	1.116	8.65	MgII	857.50	145.07
CRATES J1112+3446	11 12 38.77	+34 46 39.0	1.955	9.04	MgII CIV	2108.88	583.93
CRATES J1117+2014	11 17 06.25	+20 14 07.3	0.137	8.62	H $\alpha$ H $\beta$	1.37	1.14
B2 1144+40	11 46 58.29	+39 58 34.2	1.088	8.98	MgII	1171.13	124.91
4C +29.45	11 59 31.83	+29 14 43.8	0.724	9.18	H $\beta$ MgII	513.10	196.10
CRATES J1208+5441	12 08 54.24	+54 41 58.1	1.344	8.67	MgII	321.88	333.08
CRATES J1209+1810	12 09 51.76	+18 10 06.8	0.850	8.94	H $\beta$ MgII	288.94	40.69
4C +04.42	12 22 22.55	+04 13 15.7	0.965	8.24	MgII	720.10	169.22
4C +21.35	12 24 54.46	+21 22 46.3	0.433	8.87	H $\beta$ MgII	1617.49	29.89
CRATES J1228+4858	12 28 51.76	+48 58 01.2	1.722	9.22	MgII CIV	585.70	468.20
CRATES J1239+0443	12 39 32.75	+04 43 05.3	1.760	8.67	MgII CIV	912.84	1418.40
B2 1255+32	12 57 57.23	+32 29 29.2	0.805	8.74	H $\beta$ MgII	349.38	27.59
B2 1308+32	13 10 28.66	+32 20 43.7	0.997	8.80	MgII	837.76	497.26
B2 1315+34A	13 17 36.49	+34 25 15.8	1.054	9.29	MgII	1175.14	55.36
CGRaBS J1321+2216	13 21 11.20	+22 16 12.1	0.948	8.42	MgII	272.05	58.82
B2 1324+22	13 27 00.86	+22 10 50.1	1.403	9.24	MgII	786.65	519.85
B3 1330+476	13 32 45.23	+47 22 22.6	0.669	8.56	H $\beta$ MgII	256.41	18.89
B2 1348+30B	13 50 52.73	+30 34 53.5	0.712	8.69	H $\beta$ MgII	211.68	22.73
PKS 1434+235	14 36 40.98	+23 21 03.2	1.547	8.44	MgII CIV	595.91	110.86
PKS 1502+106	15 04 24.98	+10 29 39.1	1.839	9.64	MgII CIV	1983.07	22563.8
PKS 1509+022	15 12 15.74	+02 03 16.9	0.219	8.84	H $\alpha$ H $\beta$	10.56	3.98
PKS 1546+027	15 49 29.43	+02 37 01.1	0.414	8.61	H $\beta$ MgII	821.22	22.16
4C +05.64	15 50 35.27	+05 27 10.4	1.417	9.38	MgII	1138.94	209.33
PKS 1551+130	15 53 32.69	+12 56 51.7	1.308	9.10	MgII	1587.17	1003.15
4C +10.45	16 08 46.20	+10 29 07.7	1.231	8.64	MgII	1014.70	361.88
B2 1611+34	16 13 41.06	+34 12 47.8	1.399	9.12	MgII	3131.09	95.51
CRATES J1616+4632	16 16 03.77	+46 32 25.2	0.950	8.44	MgII	233.23	93.91
4C +38.41	16 35 15.49	+38 08 04.4	1.813	9.53	MgII CIV	5743.01	3420.04
CRATES J2118+0013	21 18 17.39	+00 13 16.7	0.462	7.93	H $\beta$ MgII	114.78	6.23
PKS 2227-08	22 29 40.08	-08 32 54.4	1.559	8.95	MgII CIV	4613.63	2464.28

**Table 1.** Sources from the DR7 Quasar Catalog that are present in the 1LAC *Fermi* sample. Col. [1]: name; Col. [2]: right ascension; Col. [3]: declination; Col. [4]: redshift; Col. [5]: Logarithm of the black hole mass (in solar masses, best estimate from S11); Col. [6]: lines measured by S11, from which  $L_{\text{BLR}}$  has been derived; Col. [7]: Broad Line Region luminosity ( $10^{42}$  erg s $^{-1}$ ), obtained from the line luminosities calculated by S11; Col. [8]:  $\gamma$ -ray luminosity from *Fermi* data ( $10^{45}$  erg s $^{-1}$ ), averaged on the first 11 months of *Fermi* operations.

of the spectra in our sample, and we excluded B3 1432+422 (SDSS J143405.69+420316.0, from the DR6 sample), because its signal-to-noise ratio was  $S/N < 5$  over the whole spectrum. Therefore, we are left with 16 DR6 objects, listed in Table 3.

In principle, the process used to derive the upper limits could be applied to the four lines measured in the work by S11 (i.e. H $\alpha$ , H $\beta$ , MgII and CIV). The objects included in the P11 sample all have  $z < 0.4$ , hence the  $\text{UL}_{\text{F}_{\text{line}}}$  can be derived only for the H $\alpha$

and H $\beta$  lines. We then derive the upper limits for these two lines. We applied the procedure also to the low redshift objects included in the DR6 sample. In 3 objects from this sample the redshift is sufficiently large to derive the upper limit on the MgII line.

Name (SDSS J...)	$z$	$\log M/M_{\odot}$	Lines	UL $L_{\text{BLR}}$ [ $10^{42} \text{ erg s}^{-1}$ ]	UL $L_{\gamma}$ [ $10^{44} \text{ erg s}^{-1}$ ]	$L_{\gamma}$ [ $10^{44} \text{ erg s}^{-1}$ ]
[1]	[2]	[3]	[4]	[5]	[6]	[7]
002200.95 +000657.9	0.306	8.49	H $\alpha$ H $\beta$	3.65	1.07	
005620.07 -093629.7	0.103	9.01	H $\alpha$ H $\beta$	1.02	0.95	
075437.07 +391047.7	0.096	8.24	H $\alpha$ H $\beta$	0.52	0.81	
080018.79 +164557.1	0.309	8.58	H $\alpha$ H $\beta$	5.68	1.09	
082323.24 +152447.9	0.167	8.80	H $\alpha$ H $\beta$	1.62	2.69	
082814.20 +415351.9	0.226	8.83	H $\alpha$ H $\beta$	2.55	5.24	
083417.58 +182501.6	0.336	9.34	H $\beta$	5.79	13.18	
083548.14 +151717.0	0.168	7.94	H $\alpha$ H $\beta$	2.87	2.75	
083918.74 +361856.1	0.335	8.50	H $\beta$	7.89	13.18	
084712.93 +113350.2	0.198	8.52	H $\alpha$ H $\beta$	3.38		3.34
085036.20 +345522.6	0.145	8.61	H $\alpha$ H $\beta$	2.07		1.74
085729.78 +062725.0	0.338	8.23	H $\beta$	7.23	13.48	
085749.80 +013530.3	0.281	8.69	H $\alpha$ H $\beta$	5.85	8.70	
090207.95 +454433.0	0.289	8.78	H $\alpha$ H $\beta$	5.24	9.33	
090314.70 +405559.8	0.188	8.28	H $\alpha$ H $\beta$	2.02	3.54	
090953.28 +310603.1	0.272	8.95	H $\alpha$ H $\beta$	6.54	8.12	
091045.30 +254812.8	0.384	8.51	H $\beta$	9.92	18.19	
091651.94 +523828.3	0.190	8.53	H $\alpha$ H $\beta$	3.07	3.63	
093037.57 +495025.6	0.187	8.48	H $\alpha$ H $\beta$	3.26	3.46	
094022.44 +614826.1	0.211	8.57	H $\alpha$ H $\beta$	3.55		11.57
094542.23 +575747.7	0.229	8.63	H $\alpha$ H $\beta$	3.23		15.97
101244.30 +422957.0	0.365	8.67	H $\beta$	13.30	15.84	
102453.63 +233234.0	0.165	7.46	H $\alpha$ H $\beta$	2.68	2.63	
102523.04 +040228.9	0.208	8.18	H $\alpha$ H $\beta$	2.74	4.36	
103317.94 +422236.3	0.211	8.59	H $\alpha$ H $\beta$	3.18	4.57	
104029.01 +094754.2	0.304	8.70	H $\alpha$ H $\beta$	6.45	10.47	
104149.15 +390119.5	0.208	8.55	H $\alpha$ H $\beta$	3.23	4.36	
104255.44 +151314.9	0.307	7.81	H $\alpha$ H $\beta$	4.56	10.71	
105344.12 +492955.9	0.140	8.47	H $\alpha$ H $\beta$	1.68		3.03
105538.62 +305251.0	0.243	8.43	H $\alpha$ H $\beta$	4.10	6.30	
105606.61 +025213.4	0.236	8.11	H $\alpha$ H $\beta$	3.43	5.88	
105723.09 +230318.7	0.378	8.32	H $\beta$	9.91	17.37	
112059.74 +014456.9	0.368	9.60	H $\beta$	9.81	16.21	
113630.09 +673704.3	0.134	8.30	H $\alpha$ H $\beta$	1.07		2.03
114023.48 +152809.7	0.244	9.46	H $\alpha$ H $\beta$	4.43	6.30	
114535.10 -034001.4	0.168	8.27	H $\alpha$ H $\beta$	2.08	2.75	
115404.55 -001009.8	0.254	8.36	H $\alpha$ H $\beta$	3.54		5.53
115709.53 +282200.7	0.300	9.20	H $\alpha$ H $\beta$	5.60	10.23	
...						

**Table 2.** BL Lacs from the work by P11. Col. [1]: SDSS name; Col. [2]: redshift; Col. [3]: Logarithm of the black hole mass (P11, in solar masses); Col. [4]: lines from which we derived the upper limits, as described in Section 3.1; Col. [5]: upper limit on the Broad Line Region luminosity ( $10^{42} \text{ erg s}^{-1}$ ), obtained from the UL on line fluxes; Col. [6]: upper limit on the  $\gamma$ -ray luminosity obtained from the *Fermi*-LAT sensitivity limit, in units of  $10^{44} \text{ erg s}^{-1}$ ; Col. [7]:  $\gamma$ -ray luminosity from *Fermi* data ( $10^{44} \text{ erg s}^{-1}$ ), averaged on the first 11 months of *Fermi* operations.

### 3.2 The distribution of black hole masses

As a byproduct of our study, we have collected (from the S11 and P11 samples) a large number of estimates for the black hole masses both in FSRQs and BL Lacs. FSRQs show a distribution skewed towards larger masses than BL Lacs:  $\langle \log M_{\text{FSRQ}} \rangle = 8.88 \pm 0.40$ ;  $\langle \log M_{\text{BL Lac}} \rangle = 8.57 \pm 0.37$ , while the average of all masses is  $\langle \log M_{\text{all}} \rangle = 8.70 \pm 0.41$ . We believe that at least in part this is due to a selection effect, since most BL Lacs come from the P11 sample, therefore they have been selected to be at  $z < 0.4$ . Assuming that very large black hole masses are rarer than smaller ones, one expects that the largest masses are found only when considering relatively large redshifts. This is illustrated by Fig. 1, that shows the black hole masses as a function of redshift for BL Lacs and FSRQs. Apart from few exceptions, the BL Lacs extend out to  $z \sim 0.4$

(by construction, given the redshift limit of the P11 sample), while FSRQs cluster around  $z \sim 1$ .

## 4 THE $L_{\text{BLR}}-L_{\gamma}$ RELATION

Fig. 2 is the key result of our work. It shows the luminosity of the BLR as a function of the observed  $\gamma$ -ray luminosity, both measured in Eddington units. Arrows correspond to upper limits. Different symbols correspond to blazars belonging to different samples, as labelled. Note that we have also added the blazars studied in G11, but omitting the objects in common. Fig. 2 shows a clear trend. Since the range in black hole masses is relatively narrow, we obtain a similar trend when plotting  $L_{\text{BLR}}$  vs  $L_{\gamma}$ . We have quantified it first by using the Kendall non-parametric test considering

Name (SDSS J...)	$z$	$\log M/M_{\odot}$	Lines	UL $L_{\text{BLR}}$ [ $10^{42}$ erg s $^{-1}$ ]	UL $L_{\gamma}$ [ $10^{44}$ erg s $^{-1}$ ]	$L_{\gamma}$ [ $10^{44}$ erg s $^{-1}$ ]
[1]	[2]	[3]	[4]	[5]	[6]	[7]
...						
120837.27 +115937.9	0.369	8.66	H $\beta$	12.56	16.21	
123123.90 +142124.4	0.256	8.62	H $\alpha$ H $\beta$	5.37	7.07	
123131.39 +641418.2	0.163	8.84	H $\alpha$ H $\beta$	1.96	2.57	
123831.24 +540651.8	0.224	8.61	H $\alpha$ H $\beta$	4.15	5.24	
125300.95 +382625.7	0.371	8.24	H $\beta$	6.81	16.59	
131330.12 +020105.9	0.356	8.50	H $\beta$	8.05	15.13	
132231.46 +134429.8	0.377	8.97	H $\beta$	9.92	17.37	
132239.31 +494336.2	0.332	8.67	H $\beta$	7.66	12.88	
132301.00 +043951.3	0.224	8.86	H $\alpha$ H $\beta$	4.23	5.24	
132617.70 +122958.7	0.204	8.63	H $\alpha$ H $\beta$	3.66	4.16	
133612.16 +231958.0	0.267	8.56	H $\alpha$ H $\beta$	4.70	7.76	
134105.10 +395945.4	0.172	8.48	H $\alpha$ H $\beta$	2.79	10.12*	
134136.23 +551437.9	0.207	8.29	H $\alpha$ H $\beta$	3.68	4.36	
134633.98 +244058.4	0.167	8.29	H $\alpha$ H $\beta$	2.42	2.69	
135314.08 +374113.9	0.216	8.79	H $\alpha$ H $\beta$	3.66	4.78	
140350.28 +243304.8	0.343	8.39	H $\beta$	7.44	13.80	
142421.17 +370552.8	0.290	8.39	H $\alpha$ H $\beta$	5.34	9.33	
142832.60 +424021.0	0.129	8.70	H $\alpha$ H $\beta$	1.90		1.86
144248.28 +120040.2	0.163	8.94	H $\alpha$ H $\beta$	2.46		3.45
144932.70 +274621.6	0.227	8.86	H $\alpha$ H $\beta$	3.77	5.37	
153311.25 +185429.1	0.307	8.91	H $\alpha$ H $\beta$	6.45	10.71	
155412.07 +241426.6	0.301	8.59	H $\alpha$ H $\beta$	5.00	10.23	
155424.12 +201125.4	0.222	8.94	H $\alpha$ H $\beta$	3.66	5.12	
160118.96 +063136.0	0.358	8.69	H $\beta$	6.78	15.13	
160519.04 +542059.9	0.212	7.85	H $\alpha$ H $\beta$	3.28	4.57	
161541.21 +471111.7	0.199	8.17	H $\alpha$ H $\beta$	3.92	3.98	
161706.32 +410647.0	0.267	7.84	H $\alpha$ H $\beta$	6.22	7.76	
162839.03 +252755.9	0.220	8.90	H $\alpha$ H $\beta$	2.71	5.01	
163726.66 +454749.0	0.192	8.42	H $\alpha$ H $\beta$	3.07	3.71	
164419.97 +454644.3	0.225	8.76	H $\alpha$ H $\beta$	4.64	5.24	
205456.85 +001537.7	0.151	8.67	H $\alpha$ H $\beta$	1.49	2.18	
205938.57 -003756.0	0.335	7.16	H $\beta$	6.61	13.18	
223301.11 +133602.0	0.214	8.54	H $\alpha$ H $\beta$	3.02	4.67	

**Table 2.** BL Lacs from the work by P11. \*: the upper limit is from the Abdo et al. (2010a) list. Col. [1]: SDSS name; Col. [2]: redshift; Col. [3]: Logarithm of the black hole mass (P11, in solar masses); Col. [4]: lines from which we derived the upper limits, as described in Section 3.1; Col. [5]: upper limit on the Broad Line Region luminosity ( $10^{42}$  erg s $^{-1}$ ), obtained from the UL on line fluxes; Col. [6]: upper limit on the  $\gamma$ -ray luminosity obtained from the *Fermi*-LAT sensitivity limit, in units of  $10^{44}$  erg s $^{-1}$ ; Col. [7]:  $\gamma$ -ray luminosity from *Fermi* data ( $10^{44}$  erg s $^{-1}$ ), averaged on the first 11 months of *Fermi* operations.

the detected sources (i.e. excluding upper limits). The Kendall  $\tau$  in this case is listed in Tab. 5. The correlation is significant both considering  $\log L_{\text{BLR}}$  vs  $\log L_{\gamma}$  and when measuring these quantities in Eddington units. Then we have considered the common dependence upon the redshifts of both luminosities, and applied the partial Kendall correlation analysis as described in Akritas & Siebert (1996). The correlation is still significant, although with a smaller  $\tau$ . We then included the upper limits, and repeating the same analysis we verify that the value of  $\tau$  is now greater.

Finally, we applied a simple least square fit and performed a partial correlation analysis (see Eq. 1 of Padovani 1992), accounting for the common dependence on the redshift and on the black hole mass of the plotted quantities. The results are listed in Tab. 5. In this case we have excluded all upper limits from the analysis.

Before discussing the implications of this correlation, there are a few caveats to remind, concerning possible important selection effects:

- In the ILAC catalog there are many detected sources without

a known redshift. As discussed in Abdo et al. (2010b) and in G11, if these sources will turn out to be at  $z \sim 2$ , then their  $\gamma$ -ray luminosities would be huge. If the absence of broad emission lines is due to their intrinsic weakness, then these blazars would be located in the bottom right part of Fig. 2, and they would be clear outliers of the found correlation. If, instead, the absence of lines is due to a particularly strong non thermal continuum, then  $L_{\text{BLR}}$  could be large, locating these objects in the “FSRQs quadrant”.

- We have clear examples of blazars varying their  $\gamma$ -ray luminosity by more than 2 orders of magnitude. It is very likely that the present samples of  $\gamma$ -ray detected blazars preferentially include objects in their high state<sup>1</sup>. The  $\gamma$ -ray luminosity we have considered is the average over 11 months (therefore the short term variability is

<sup>1</sup> This would also explain why the radio and  $\gamma$ -ray fluxes are correlated, even if only a relatively small fraction of radio-loud AGN with a flat spectrum are detected in  $\gamma$ -rays; see e.g. Ghirlanda et al. (2011).

Name	RA	DEC	$z$	Lines	UL $L_{\text{BLR}}$ [ $10^{42}$ erg s $^{-1}$ ]	$L_{\text{BLR}}$ [ $10^{42}$ erg s $^{-1}$ ]	$L_{\gamma}$ [ $10^{45}$ erg s $^{-1}$ ]
[1]	[2]	[3]	[4]	[5]	[6]	[7]	[8]
B2 0806+35	08 09 38.87	+34 55 37.2	0.082	H $\alpha$ H $\beta$	0.49		0.18
CRATES J0809+5218	08 09 49.18	+52 18 58.2	0.138	H $\alpha$ H $\beta$	7.581		1.45
Ton 1015	09 10 37.03	+33 29 24.4	0.354	H $\alpha$ H $\beta$	30.675		4.54
CRATES J1012+0630	10 12 13.34	+06 30 57.2	0.727	H $\beta$ MgII	134.295		35.9
1ES 1011+496	10 15 04.14	+49 26 00.6	0.212	H $\beta$	19.9		9.72
B2 1040+24A	10 43 09.04	+24 08 35.4	0.560	MgII		25.4	13.7
PKS 1055+01	10 58 29.60	+01 33 58.8	0.890	MgII		131.8	377.2
CGRaBS J1058+5628	10 58 37.73	+56 28 11.1	0.143	H $\alpha$ H $\beta$	3.85		3.58
PKS 1106+023 <sup>a</sup>	11 08 45.48	+02 02 40.8	0.157	H $\beta$		4.7	0.51
1ES 1118+424	11 20 48.06	+42 12 12.4	0.124	H $\alpha$ H $\beta$	1.797		0.47
B2 1147+24	11 50 19.21	+24 17 53.8	0.200	H $\alpha$ H $\beta$	9.627		1.47
B2 1218+30	12 21 21.94	+30 10 37.2	0.184	H $\alpha$ H $\beta$	6.04		3.34
W Com	12 21 31.69	+28 13 58.4	0.102	H $\alpha$ H $\beta$	5.26		1.80
B2 1229+29	12 31 43.57	+28 47 49.7	0.236	H $\alpha$ H $\beta$	9.696		4.31
CRATES J1253+0326	12 53 47.00	+03 26 30.3	0.066	H $\alpha$ H $\beta$	0.41		0.13
PG 1437+398	14 39 17.47	+39 32 42.8	0.344	H $\alpha$ H $\beta$	17.93		4.27

**Table 3.** Sources from the DR6 Catalog that are present in the 1LAC Fermi sample. Col. [1]: name; Col. [2]: right ascension; Col. [3]: declination; Col. [4]: redshift; Col. [5]: lines measured or for which we derived the upper limits as described in Section 3.1; Col. [6]: upper limit on the Broad Line Region luminosity ( $10^{42}$  erg s $^{-1}$ ), obtained from the UL on line fluxes; Col. [7]: luminosity of the Broad Line region ( $10^{42}$  erg s $^{-1}$ ); Col. [8]:  $\gamma$ -ray luminosity from *Fermi* data ( $10^{45}$  erg s $^{-1}$ ), averaged on the first 11 months of *Fermi* operations. The black masses are not available, hence a medium mass value ( $M = 5 \times 10^8 M_{\odot}$ ) has been assigned to all of them. <sup>a</sup>: PKS 1106+023 has the H $\beta$  line measured in DR6 Catalog, hence its mass can be estimated by the Chiaberge & Marconi relation (2011): a value of  $M=4 \times 10^7 M_{\odot}$  is obtained.

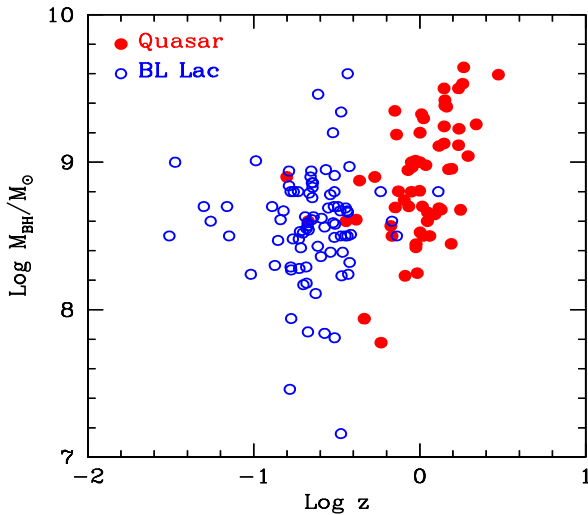


**Figure 1.** Black hole masses as a function of redshift. Empty circles are BL Lacs, filled circles are FSRQs. BL Lacs of our sample have significantly smaller redshift than FSRQs.

averaged for), but blazars can indeed be variable over longer periods. This variability introduces an inevitable dispersion around the correlation line.

- Misaligned jets should be weaker  $\gamma$ -ray sources than their aligned counterpart, but they would show the same emission line luminosities. Therefore weak  $\gamma$ -ray sources *must* exist, populating the region to the left of the interpolating line of Fig. 2. However, these sources would be classified as radio-galaxies (see Abdo et al. 2010c), and not aligned blazars, although some overlap might exist.

Despite the presence of the above caveats, the apparent cor-

relation between the BLR and the jet  $\gamma$ -ray luminosity is certainly intriguing, since it would prove the importance of the emission line photons in the production of high energy  $\gamma$ -rays and, more importantly, it would point towards a relation between the accretion rate and the jet power. This relation is not direct, however, since the observed  $\gamma$ -ray luminosity can be considered a rather poor proxy of the jet power and the disc luminosity is linearly related to the accretion rate only for “standard” optically thick geometrically thin accretion disc. This will be discussed more in the next section.

Fig. 2 shows that BL Lac objects are rather neatly divided from FSRQs: with few exceptions, all FSRQs have  $L_{\text{BLR}}/L_{\text{Edd}} > 5 \times 10^{-4}$  and all BL Lacs are below this value. The corresponding dividing  $\gamma$ -ray luminosity is  $L_{\gamma}/L_{\text{Edd}} \sim 0.1$ . We derived this apparent “divide” considering only the sources for which we have a detection of the BLR and the  $\gamma$ -ray luminosities. In other words, we first excluded the upper limits from the analysis. The paucity of data does not allow us to reach a firm conclusion about the exact value of this divide, but, reassuringly, when we include all the upper limits they lie in the “correct” quadrant of the plane.

On the other hand, most upper limits correspond to BL Lacs with  $z < 0.4$ , so an issue remains: the divide between BL Lacs and FSRQs could be partly due to a segregation in redshift, if all BL Lacs are at low redshift and FSRQs at high redshift. To verify this, we plot in Fig. 3 the BLR luminosity (in Eddington units) as a function of redshift. It can be seen that there are *detected* BL Lacs with  $L_{\text{BLR}}/L_{\text{Edd}} < 5 \times 10^{-4}$  at relatively large redshifts. This is a hint that the divide is real, but, again, the paucity of points precludes a firmer conclusion about this possible selection effect. Moreover, most of the upper limits come from the P11 sample, that by construction selects only BL Lacs at  $z < 0.4$ . This limit in redshift possibly introduces a bias in the dividing value, as can be seen in Fig 3. Nevertheless, we reiterate that the upper limits did not

Name	RA	DEC	$z$	$\log M/M_{\odot}$	$L_{\text{BLR}}$ [ $10^{42} \text{ erg s}^{-1}$ ]	$L_{\gamma}$ [ $10^{45} \text{ erg s}^{-1}$ ]
[1]	[2]	[3]	[4]	[5]	[6]	[7]
<b>‘FS’</b>						
PKS 0208-512	02 11 13.18	+10 51 34.8	1.003	9.2	3700	489.8
PKS 0235+164	02 38 38.93	+16 36 59.3	0.940	9.0	100	1737.8
PKS 0426-380	04 28 40.42	-37 56 19.6	1.111	8.6	110	1513.6
PKS 0537-441	05 38 50.35	-44 05 08.7	0.892	8.8	690	1000.0
PKS 0808+019	08 11 26.71	+01 46 52.2	1.148	8.5	42	120.2
<b>LBL</b>						
PKS 0521-36	05 22 57.98	-36 27 30.9	0.055	8.6	4.8	0.28
PKS 0829+046	08 31 48.88	+04 29 39.1	0.174	8.8	3.7	2.45
OJ 287	08 54 48.87	+20 06 30.6	0.306	8.8	6.8	1.51
TXS 0954+658	09 58 47.25	+65 33 54.8	0.367	8.5	2.8	4.90
PMN 1012+0630	10 12 13.35	+06 30 57.2	0.727	8.5	7.8	35.5
PKS 1057-79	10 58 43.40	-80 03 54.2	0.581	8.8	58	45.7
PKS 1519-273	15 22 37.68	-27 30 10.8	1.294	8.8	34	354.8
PKS 1749+096	17 51 32.82	+09 39 00.7	0.322	8.7	50	26.9
S5 1803+78	18 00 45.68	+78 28 04.0	0.680	8.6	710	87.1
3C 371	18 06 50.68	+69 49 28.1	0.050	8.7	1.0	0.19
BL Lac	22 02 43.29	+42 16 40.0	0.069	8.7	3.3	0.93
PKS 2240-260	22 43 26.47	-25 44 31.4	0.774	8.6	29	56.23
<b>HBL</b>						
Mkn 421	11 04 27.30	+38 12 32.0	0.031	8.5	0.5	0.33
Mkn 501	16 53 52.20	+39 45 37.0	0.034	9.0	1.6	0.09
PKS 2005-489	20 09 25.40	-48 49 54.0	0.071	8.5	1.1	0.32
WGA 1204.2-0710	12 04 16.66	-07 10 09.0	0.185	8.8	<9.5	0.98
<b>FSRQ</b>						
TXS 1013+054	10 16 03.10	+05 13 02.0	1.713	9.5	889	1584.9
S4 1030+61	10 33 51.40	+60 51 07.3	1.401	9.5	450	741.31
PKS 1144-379	11 47 01.40	-38 12 11.0	1.049	8.5	400	223.9
3C 273	12 29 06.69	+02 03 08.5	0.158	8.9	3380	21.4
3C 279	12 56 11.10	-05 47 21.5	0.536	8.9	242	204.2
PKS 1510-089	15 12 50.50	-09 06 00.0	0.360	8.6	741	125.9
OX 169	21 43 35.50	+17 43 48.6	0.213	8.6	182	8.51
CTA102	22 32 36.40	+11 43 53.8	1.037	8.7	4140	489.8
3C 454.3	22 53 57.70	+16 08 53.6	0.859	8.7	3330	5011.9

**Table 4.** Blazars from G11. Col. [1]: name; Col. [2]: right ascension; Col. [3]: declination; Col. [4]: redshift; Col. [5]: Logarithm of the black hole mass (in solar masses); Col. [6]: Broad Line Region luminosity ( $10^{42} \text{ erg s}^{-1}$ ); Col. [7]:  $\gamma$ -ray luminosity ( $10^{45} \text{ erg s}^{-1}$ ).

take part in the determination of the divide, hence this bias does not completely compromise the result.

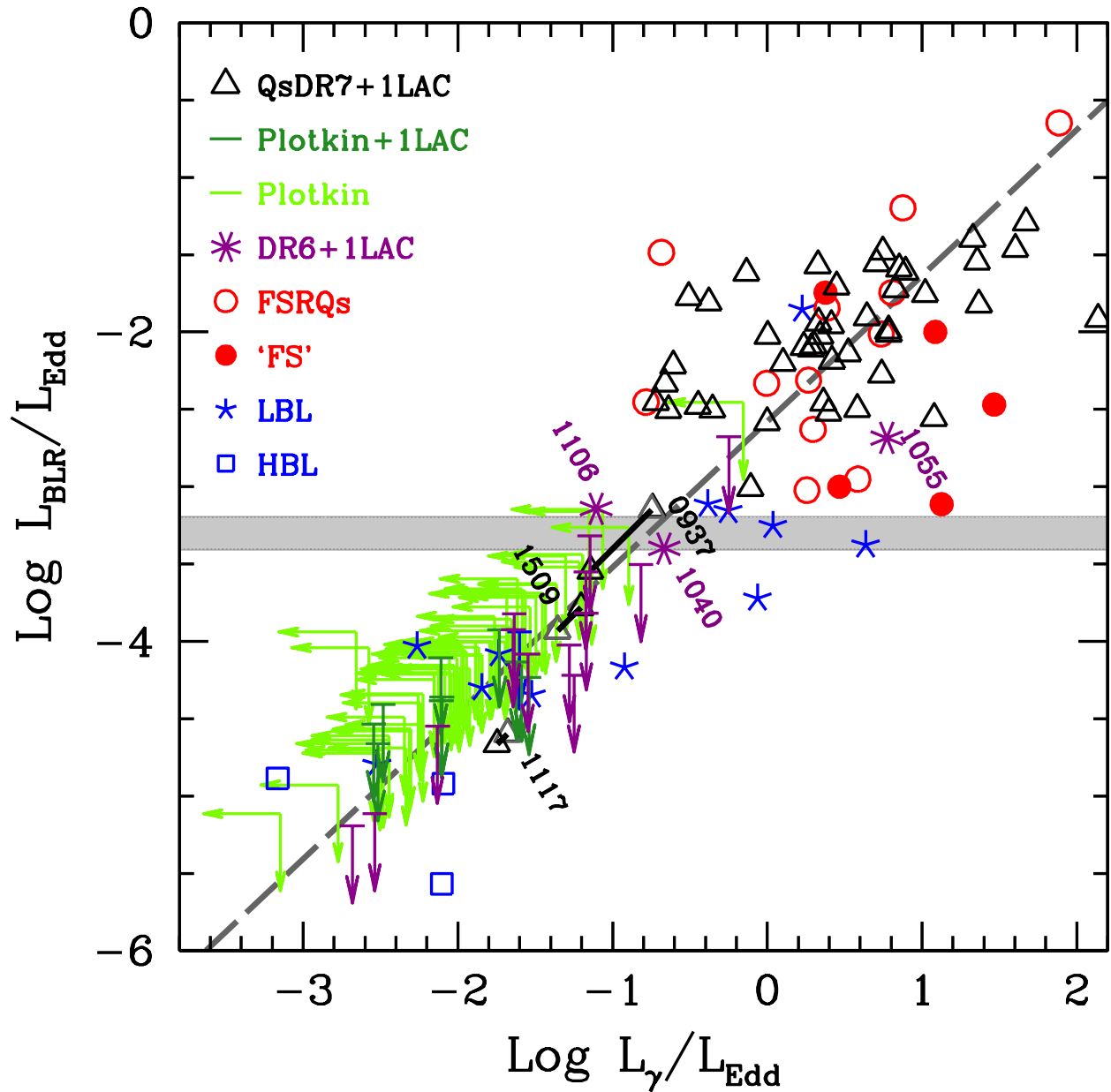
If real, the found divide would be in agreement with what found studying the distribution of bright *Fermi* detected blazars in the  $\gamma$ -ray spectral index –  $\gamma$ -ray luminosity plane (for them Ghisellini Maraschi & Tavecchio 2009 proposed a “divide” between BL Lacs and FSRQs around  $L_d/L_{\text{Edd}} \sim 10^{-2}$ ), and to what more recently found by G11 using a sample of bright blazars much more limited in number than what we use here. The value of the divide found here would also be consistent with the division between FR I and FR II radio–galaxies, found with a completely different approach by Ghisellini & Celotti (2001).

Fig. 2 shows also that all blazars form a continuous family, with no apparent “discontinuity” (or sign of bimodality). Excluding upper limits, we find that  $L_{\text{BLR}} \propto L_{\gamma}$  (normalizing or not to Eddington). One can then wonder if it is still meaningful to divide BL Lac objects from FSRQs, since in Fig. 2 they form a continuous distribution. In other words: are BL Lacs and FSRQs characterized

by some different fundamental properties, or are they simply at two sides of a continuous distribution of properties? An example can illustrate this point: suppose, as suggested by Ghisellini, Maraschi & Tavecchio (2009) that the accretion disc in BL Lacs is radiatively inefficient, while it is efficient in FSRQs. This is a fundamental different property, although it concerns the accretion disc, not the jet. Another example: suppose that jets in BL Lacs are made by pure electron–positron plasmas, while the jets in FSRQs are made by normal electron–proton plasmas. This, too, should be considered a fundamental different property. If instead all blazars have radiatively efficient accretion disc and their jets are all made by electrons and protons, then they *look* different only because they have different overall powers, and this in turn might also explain why their SED is different, without the need of anything fundamental dividing them.

The discussion below is dedicated to this issue, focussing in particular to the proposed “divide” of BL Lacs and FSRQs in terms of the mass accretion rate in Eddington units.





**Figure 2.** Luminosity of the broad line region (in Eddington units) for the sources from our samples and from G11 as a function of the  $\gamma$ -ray luminosity (in Eddington units). Different symbols correspond to different samples or a different classification of the sources, as labelled. The three (violet) asterisks are the only sources with visible broad emission lines from the DR6 *Fermi* detected sample. The three labelled triangles have their synchrotron emission dominating over the thermal emission in their SEDs. Hence, to avoid black hole mass estimate errors, possibly occurred in the S11 automatic calculation, we also assigned them an average  $M_{\text{BH}}$  value ( $M_{\text{BH}} = 5 \times 10^8 M_{\odot}$ ). These changes are highlighted by the thick (black) segments ending to the black triangles (corresponding to the average  $M_{\text{BH}}$  value). The grey stripe indicates the luminosity “divide” between FSRQs and BL Lacs at  $L_{\text{BLR}}/L_{\text{Edd}} \sim 5 \times 10^{-4}$ .

## 5 DISCUSSION

Our study concerns  $L_{\text{BLR}}$ ,  $L_{\gamma}$ , and the black hole mass. In the following we will discuss how we can use  $L_{\text{BLR}}$  to find the disc luminosity  $L_{\text{d}}$ , and how to use  $L_{\gamma}$  to find a proxy for the jet power  $P_{\text{jet}}$  and the mass accretion rate  $\dot{M}$ . The black hole mass is of course used to normalize all powers to the Eddington luminosity.

$$L_{\text{BLR}} \rightarrow L_{\text{d}} \rightarrow \dot{M} \text{ — For radiatively efficient accretion}$$

discs, the BLR luminosity is a direct measure of the disc luminosity  $L_{\text{d}}$ , since, on average,  $L_{\text{d}} \sim 10 L_{\text{BLR}}$  (see e.g. Baldwin & Netzer 1978; Smith et al. 1981). Radiatively efficient (i.e. Shakura–Sunjaev 1973) disc should occur for  $\dot{m} \equiv \dot{M}/\dot{M}_{\text{Edd}} > \dot{m}_{\text{c}}$ . Defining  $\dot{M}_{\text{Edd}} \equiv L_{\text{Edd}}/c^2$  (without the efficiency factor), then  $\dot{m}_{\text{c}}$  should be close to 0.1 (Narayan & Yi, 1995). Another hypothesis suggests the lower value  $\dot{m}_{\text{c}} \sim 10^{-4}$  for the radiative transition (Sharma et al. 2007). If the disc emits as a black-body at all radii,

Kendall	$\tau$				
	detections	det.+UL			
$\log L_{\text{BLR}} - \log L_\gamma$	0.530	0.561			
$\log L_{\text{BLR}} - \log L_\gamma, z$	0.281	0.386			
$\log(L_{\text{BLR}}/L_{\text{Edd}}) - \log(L_\gamma/L_{\text{Edd}})$	0.398	0.529			
$\log(L_{\text{BLR}}/L_{\text{Edd}}) - \log(L_\gamma/L_{\text{Edd}}), z$	0.266	0.376			
Minimum square fit (only det.)	$m$	$q$	$N$	$r$	$P$
$\log L_{\text{BLR}} - \log L_\gamma$	0.93	0.61	78	0.83	$< 4 \times 10^{-8}$
$\log L_{\text{BLR}} - \log L_\gamma, z$	0.93	0.61	78	0.64	$< 4 \times 10^{-8}$
$\log(L_{\text{BLR}}/L_{\text{Edd}}) - \log(L_\gamma/L_{\text{Edd}})$	0.94	-2.58	78	0.78	$< 4 \times 10^{-8}$
$\log(L_{\text{BLR}}/L_{\text{Edd}}) - \log(L_\gamma/L_{\text{Edd}}), z$	0.94	-2.58	78	0.67	$< 4 \times 10^{-8}$
$\log(L_{\text{BLR}}/L_{\text{Edd}}) - \log(L_\gamma/L_{\text{Edd}}), z, M$	0.94	-2.58	78	0.64	$< 4 \times 10^{-8}$

**Table 5.** The first part of the table reports the results of the non-parametric Kendall test for the complete sample, taking into consideration at first only the sources with both  $L_{\text{BLR}}$  and  $L_\gamma$  detected, then including upper limits. We list also the results when accounting for the common dependence on redshift. The bottom part of the table reports the results of a partial correlation analysis using a least square fit. We have excluded upper limits from the analysis. Correlations are of the form  $\log y = m \log x + q$ . The listed slopes  $m$  refer to the bisector (of the two correlations  $x$  vs  $y$  and  $y$  vs  $x$ ).  $N$  is the total number of objects.  $r$  is the correlation coefficient obtained from the analysis.  $P$  is the probability that the correlation is random.

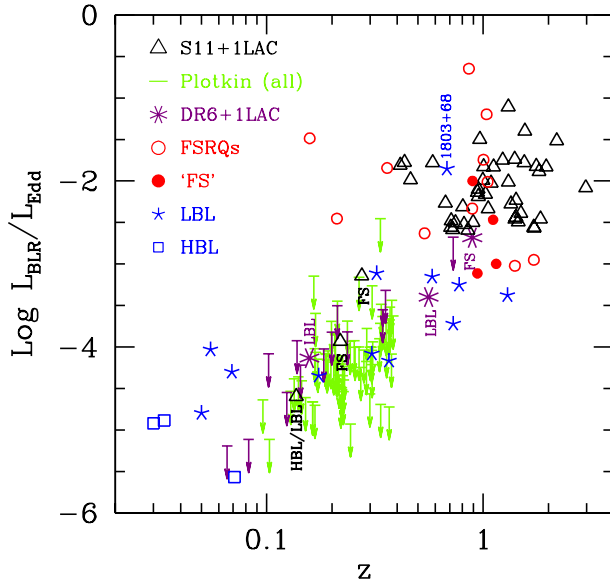


**Figure 3.** The broad line luminosity (in Eddington units) as a function of redshift. Same symbols as in Fig. 2.

then most of the power is emitted in the far UV, and we can approximate the photo-ionizing luminosity with the entire  $L_d$ .

When  $\dot{m} < \dot{m}_c$ , the disc should become radiatively inefficient, because the particle density of the accretion flow becomes small, and the energy exchange timescale between protons and electrons becomes smaller than the accretion time. If this occurs, the disc bolometric luminosity decreases. Narayan, Garcia & McClintock (1997) proposed that in this regime  $L_d \propto \dot{M}^2$ . In this case the disc becomes hot, inflates, and it does not emit black-body radiation. As a consequence,  $L_{\text{ion}} \ll L_d$ . According to Mahadevan (1997, see his Fig. 1), the decreasing fraction of the ionizing luminosity is as important as the decrease of the overall efficiency  $\eta$  (defined as  $L_d = \eta \dot{M} c^2$ ). In the example shown by Fig. 1 of Mahadevan (1997),  $L_{\text{ion}} \propto \dot{M}^{3.5}$ . If this were true, we expect also the broad emission line luminosity to have the same dependence on  $\dot{M}$

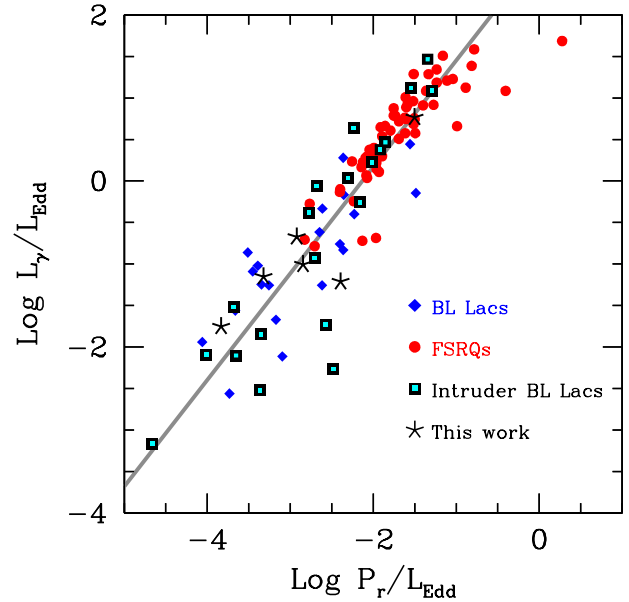


**Figure 4.** The  $\gamma$ -ray luminosity in the LAT band as a function of the jet power  $P_r$  (both in Eddington units). The latter is the power that the jet has spent to produce the (bolometric) radiation we see, and is given by  $P_r \sim L_{\text{bol}}/\Gamma^2$ . To derive it we have used blazars detected by *Fermi* for which we have constructed the SED and estimated the bulk Lorentz factor (G10; G11; Tavecchio et al. 2010). The grey solid line shows the result (bisector) of a least square fit.

when  $\dot{M}$  goes sub-critical. Note, however, that the SED calculated by Mahadevan (1997) could be largely affected by the presence of extra sources of seed photons for the thermal Comptonization, besides the assumed cyclotron-synchrotron emission. These extra seed photons (for instance coming from some cool part of the disc) could enhance the UV emission both by enhancing the Compton scattering and by cooling the hot emitting electrons. So we regard the  $L_{\text{BLR}} \propto L_{\text{ion}} \propto \dot{M}^{3.5}$  relation as an indication, but without excluding other possibilities. In practice, for  $\dot{m} < \dot{m}_c$ , we will consider both  $L_{\text{BLR}} \propto \dot{M}^2$  and  $L_{\text{BLR}} \propto \dot{M}^{3.5}$ .

$L_\gamma \rightarrow P_{\text{jet}} \rightarrow \dot{M}$  — A lower limit on the jet power  $P_{\text{jet}}$  is

$$P_{\text{jet}} > P_r \gtrsim \frac{L_{\text{bol}}}{\Gamma^2} \quad (1)$$

where  $\Gamma$  is the bulk Lorentz factor (see Celotti & Ghisellini 2008 and Ghisellini & Tavecchio 2009),  $L_{\text{bol}}$  is the jet bolometric luminosity, measured assuming isotropic emission.  $P_r$  is the power that the jet has to spend to produce the radiation we see. If  $P_{\text{jet}} \sim P_r$ , then the jet uses its entire power to produce radiation, including its kinetic power, and it should stop. Fitting the SED of a large number of blazars detected by *Fermi* with a simple one-zone leptonic model (as the one used in the Appendix) returns values of  $\Gamma$  contained in a narrow range, around 13–15 (see Ghisellini et al. 2010; hereafter G10), consistent with the values one derives from the superluminal motion. The same model also yields the number of emitting electrons required to account for the radiation we see, and by assuming one proton per electron, it yields  $P_{\text{jet}} \sim 30\text{--}100P_r$ , on average. We can conclude that  $P_{\text{jet}}$  is robustly bound to be larger than  $P_r \sim L_{\text{bol}}/200$  and it can be a factor 30–100 larger than that.

The key result obtained in G10 (confirming earlier results in Celotti & Ghisellini 2008 and then also confirmed by G11), is that  $P_{\text{jet}} \sim \dot{M}c^2$ . Since  $P_r$  is linearly related to  $P_{\text{jet}}$ , and it is a model-independent quantity, we can safely use  $P_r$  as a proxy for  $P_{\text{jet}}$  and  $\dot{M}$ . To measure  $P_r \sim L_{\text{bol}}/\Gamma^2$  we should construct the SED of all our blazars. On the other hand, we can take advantage from the sample already studied in the literature, to find if there is a robust relation between  $P_r$  and the  $\gamma$ -ray luminosity  $L_\gamma$  in the *Fermi*/LAT energy range, that is the quantity most readily available to us. Such a robust relation indeed exists, and it is shown in Fig. 4. Fitting it with a simple least square method and taking the bisector we obtain:

$$\text{Log} \left( \frac{L_\gamma}{L_{\text{Edd}}} \right) = 1.284 \text{Log} \left( \frac{P_r}{L_{\text{Edd}}} \right) + 2.738 \quad (2)$$

Note that the two quantities are not linearly related. At low values of  $L_\gamma/L_{\text{Edd}}$ , the  $\gamma$ -ray luminosity *underestimate*  $P_r$  (either normalizing or not to the Eddington luminosity). As a consequence, the  $L_\gamma/L_{\text{Edd}}$  values for low luminosity BL Lacs underestimate the jet power, and in turn the mass accretion rate. This occurs because  $L_\gamma$  is not a good indicator of  $L_{\text{bol}}$  for low luminosity BL Lacs, that have their high energy SED peaking in the TeV band, and that have an important (often dominant) synchrotron component.

$L_{\text{BLR}}/L_{\text{Edd}}$  vs  $P_r/L_{\text{Edd}}$  — Since the above correlation appears rather robust, we can use it to obtain  $P_r/L_{\text{Edd}}$  from our values of  $L_\gamma$  and black hole mass, without the need to construct the SED and modelling it. In turn, we can think at the obtained  $P_r/L_{\text{Edd}}$  values as proportional to the mass accretion rate in Eddington units. This is done in Fig. 5 where we plot  $L_{\text{BLR}}/L_{\text{Edd}}$  as a function of  $P_r/L_{\text{Edd}}$ .

For  $\dot{m} > \dot{m}_c$ , we expect that the BLR luminosity, in Eddington units, depends linearly on the normalized accretion rate, and therefore  $L_{\text{BLR}}/L_{\text{Edd}} \propto \dot{m} \propto P_r/L_{\text{Edd}}$ .

Below  $\dot{m} \sim \dot{m}_c$ , we expect that the disc becomes radiatively inefficient. The disc *bolometric* luminosity becomes proportional to  $\dot{m}^2$ , while the *ionizing* luminosity can follow an even steeper relation with  $\dot{m}$  (i.e.  $\propto \dot{m}^{3.5}$ , see above). The grey stripe at small  $L_{\text{BLR}}/L_{\text{Edd}}$  is proportional to  $P_r/L_{\text{Edd}}$  in the top panel, to  $(P_r/L_{\text{Edd}})^2$  in the mid panel and to  $(P_r/L_{\text{Edd}})^{3.5}$  in the bottom panel. We mainly consider the Narayan & Yi hypothesis of  $m_c \sim 0.1$ . The break value has been chosen to correspond to  $L_{\text{BLR}}/L_{\text{Edd}} \sim 5 \times 10^{-4}$ , and allowing for considerable scatter around this value. Note that, if we take into account the  $m_c \sim 10^{-4}$

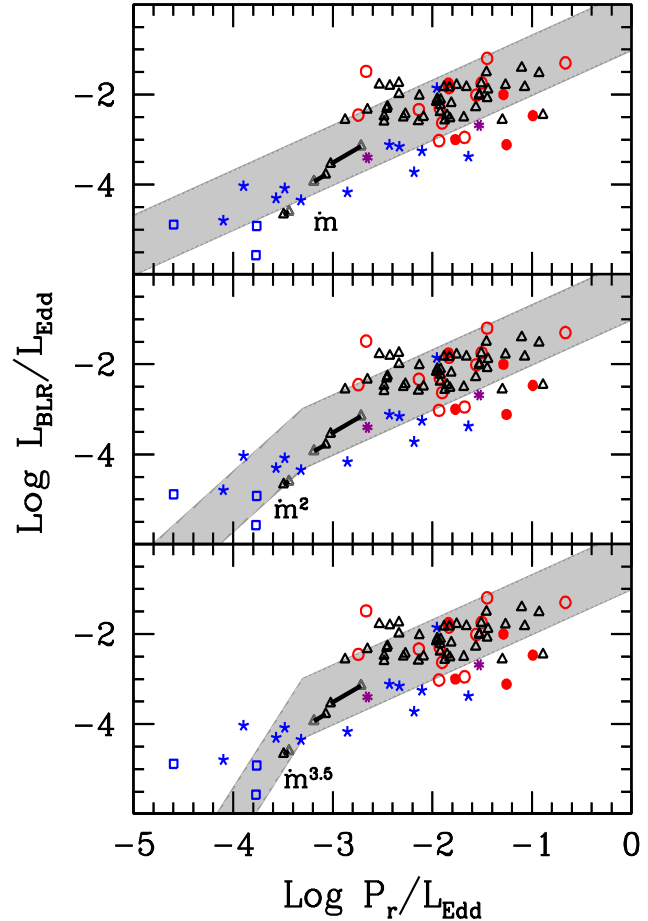


**Figure 5.** Luminosity of the broad line region (in Eddington units) for the sources from our samples and from G11 as a function of  $P_r$  (in Eddington units). Symbols are the same as Fig. 2, but without upper limits and with grey stripes superimposed. In all three panels we assume that  $P_r$  tracks  $\dot{M}$ . If this is true, we can see how the broad line luminosity is related to  $\dot{m} \equiv \dot{M}/\dot{M}_{\text{Edd}}$ , or, equivalently, to  $P_r/L_{\text{Edd}}$ . At large values of  $L_{\text{BLR}}/L_{\text{Edd}}$  the grey stripe of all panels corresponds to  $L_{\text{BLR}}/L_{\text{Edd}} \propto P_r/L_{\text{Edd}}$ . In the top panel the grey stripe continues to show a linear relation also at low values of  $L_{\text{BLR}}/L_{\text{Edd}}$ , while in the mid panel the grey stripe becomes quadratic below some critical value (here  $L_\gamma/L_{\text{Edd}} = 0.1$  is assumed, namely the value dividing BL Lacs from FSRQs). In the bottom panel, the grey stripe becomes  $L_{\text{BLR}}/L_{\text{Edd}} \propto (P_r/L_{\text{Edd}})^{3.5}$  at low values, to account for the deficit of ionizing UV photons in radiatively inefficient disc.

hypothesis (Sharma et al. 2007), the break values would be outside the luminosity range of our sample.

Fig. 5 shows that we cannot yet distinguish among the different cases, even if there is some preference for the  $L_{\text{BLR}}/L_{\text{Edd}} \propto (P_r/L_{\text{Edd}})^2$  case.

There are BL Lacs of the HBL type, such as Mkn 421, Mkn 501 and 2005–489, that do show broad emission lines (and the prototypical BL Lac object too, i.e. BL Lac itself), with  $L_{\text{BLR}}$  around  $10^{42} \text{ erg s}^{-1}$  and  $L_{\text{BLR}}/L_{\text{Edd}}$  around  $10^{-5}$ . These are the objects at the low (bottom-left) end of Fig. 2, Fig. 4 and Fig. 5. We need more low power BL Lacs to investigate if they are indeed associated with radiatively inefficient discs.

*Note that this is not required* by the basic explanation of the blazar sequence and by the proposed luminosity “divide” between BL Lacs and FSRQs. In fact, the change of the observed SED along the blazar sequence, interpreted as a radiatively cooling sequence

(Ghisellini et al. 1998), requires that in BL Lacs the emission lines are not important as seed photons for the inverse Compton process. This can be the case *even if the lines are present*, if the dissipation region occurs outside  $R_{\text{BLR}}$ : in this case the BLR photons are seen in the comoving region red-shifted and time-diluted, and the EC process can be negligible. The relation between the size of the BLR and the ionizing luminosity ensures that in BL Lacs the size of the BLR is much smaller than in FSRQs, even if the black hole mass is similar. If dissipation occurs always at  $R_{\text{diss}} \sim 10^3$  Schwarzschild radii, then in BL Lacs we easily have  $R_{\text{diss}} > R_{\text{BLR}}$  (and emitting lines are negligible for the formation of the high energy spectrum), while in more powerful FSRQs we have  $R_{\text{diss}} < R_{\text{BLR}}$ , with a corresponding enhancement of the EC process. Earlier works (Celotti & Ghisellini 2008; G10, G11) have shown that  $R_{\text{diss}}$  is of the order of  $\sim 10^3$  Schwarzschild radii in all objects. Requiring that the size of the BLR is a factor  $f$  smaller than this, and using  $R_{\text{BLR}} = 10^{17} L_{\text{d},45}^{1/2}$  cm, we obtain

$$R_{\text{BLR}} < f R_{\text{diss}} \rightarrow \frac{L_{\text{d}}}{L_{\text{Edd}}} < 6.9 \times 10^{-3} f^2 M_8 \left( \frac{R_{\text{diss}}}{10^3 R_{\text{S}}} \right)^2 \quad (3)$$

where  $M = 10^8 M_8$  solar masses. We obtain, in this case, a value for the divide in agreement with the observed  $L_{\text{BLR}}/L_{\text{Edd}} \sim 5 \times 10^{-4}$  (for  $L_{\text{BLR}} \sim 0.1 L_{\text{d}}$  and  $f$  smaller than, but close to unity), but dependent on the black hole mass. The dependence on the black hole mass would produce some blur in the division, that is not inconsistent with what we see.

## 6 CONCLUSIONS

In this work we have studied those blazars detected by *Fermi*/LAT and present in the SDSS optical survey, for which the redshift is known and there is a black hole mass estimate. From the broad emission line luminosities (or their upper limits) we have calculated the luminosity of the entire Broad Line Region, used as a proxy for the luminosity of the accretions disc. We could find values for both the BLR and the  $\gamma$ -ray luminosity for 78 blazars, values for  $L_{\text{BLR}}$  and upper limits on  $L_{\gamma}$  for 23 blazars, and upper limits on both the quantities for 62 sources. Our results can be summarized as follows:

- (i) The luminosity of the BLR correlates well with the  $\gamma$ -ray luminosity in the *Fermi*/LAT energy range. The correlation is linear, irrespective if the above luminosities are normalized to Eddington or not. All upper limits (not used to find the correlation) are consistent with the correlation itself.
- (ii) BL Lac objects and FSRQs occupy different regions of the  $L_{\text{BLR}}/L_{\text{Edd}} - L_{\gamma}/L_{\text{Edd}}$  plane, with a division at about  $L_{\text{BLR}}/L_{\text{Edd}} \sim 5 \times 10^{-4}$ . This confirms, with an enlarged sample, earlier results. Nevertheless, since the sample is still rather poor of sources with detections on both  $L_{\text{BLR}}$  and  $L_{\gamma}$  and instead rich of upper limits, this “divide” still needs further studies with a more populated sample.
- (iii) For objects (analyzed in previous works) of known  $L_{\gamma}$ ,  $P_{\text{r}}$ , and black hole mass, there is a strong correlation between the two quantities, both using absolute values and normalizing them to the Eddington luminosity:  $(L_{\gamma}/L_{\text{Edd}}) \propto (P_{\text{r}}/L_{\text{Edd}})^{1.28}$ . As a consequence, the  $\gamma$ -ray luminosity (in the *Fermi*/LAT energy range) can be used to estimate  $P_{\text{r}}$  which is a robust proxy for the jet power.
- (iv) The relation between the strength of the emission lines and the accretion rate can be used to test radiatively inefficient disc models and the prediction about the production, in these discs, of

the ionizing luminosity. Our results are too primitive to draw strong conclusions, but there is the possibility that at low accretion rates the produced ionizing UV luminosity is larger than expected.

- (v) The division between BL Lacs and FSRQs could be due to the transition between a radiatively inefficient disc to a standard (Shakura–Sunyaev) disc. Alternatively, it can be due to the dissipation region of the jet being located outside or inside the BLR.

## ACKNOWLEDGMENTS

We thank the referee for useful comments that improved the paper. We thank Julian Krolik for suggesting us the possibility of a transition to ADAF at accretion rates smaller than what we considered. We also thank F. Tavecchio, G. Ghirlanda and L. Foschini for discussions. This research made use of the NASA/IPAC Extragalactic Database (NED) which is operated by the Jet Propulsion Laboratory, Caltech, under contract with NASA, and of the *Swift* public data made available by the HEASARC archive system.

## REFERENCES

- Abdo A.A., Ackermann M., Ajello M. et al., 2009, ApJ, 700, 597
- Abdo A.A., Ackermann M., Ajello M. et al., 2010a, ApJ, 715, 429
- Abdo A.A., Ackermann M., Agudo I. et al., 2010b, ApJ, 716, 30
- Abdo A.A., Ackermann M., Ajello M. et al., 2010c, ApJ, 720, 912
- Ackermann M., Ajello M., Allafort A., et al., 2011, ApJ subm. (astro-ph/1108.1420)
- Adelman-McCarthy J.K., Agüeros M.A., Allam S.S. et al., 2008, ApJS, 175, 297
- Akritas M.G. & Siebert J., 1996, MNRAS, 278, 919
- Baldwin J.A. & Netzer H., 1978, ApJ, 226, 1
- Celotti A., Padovani P., & Ghisellini G., 1997, MNRAS, 286, 415
- Celotti A. & Ghisellini G., 2008, MNRAS, 385, 283
- Chiaberge M. & Marconi A., 2011, MNRAS, in press (astro-ph/1105.4889)
- Condon J.J., Cotton W.D., Greisen E.W., Yin Q.F., Perley R.A., Taylor G.B. & Broderick J.J., 1998, AJ, 115, 1693
- Decarli R., Dotti M. & Treves A., 2011, MNRAS, 413, 39
- D’Elia V., Padovani P. & Landt H., 2003, MNRAS, 339, 1081
- Francis P.J., Hewett P.C., Foltz C.B., Chaffee F.H., Weymann R.J. & Morris S.L., 1991, ApJ, 373, 465
- Ghirlanda G., Ghisellini G., Tavecchio F., Foschini L. & Bonnoli G., 2011, MNRAS, 413, 852
- Ghisellini G., Celotti A., Fossati G., Maraschi L. & Comastri A., 1998, MNRAS, 301, 451
- Ghisellini G. & Celotti A., 2001, A&A, 379, L1
- Ghisellini G., Maraschi L. & Tavecchio F., 2009, MNRAS, 396, L105
- Ghisellini G. & Tavecchio F., 2009, MNRAS, 397, 985
- Ghisellini G., Tavecchio F., Foschini L., Ghirlanda G., Maraschi L. & Celotti A., 2010, MNRAS, 402, 497 (G10)
- Ghisellini G., Tavecchio F., Foschini L., Ghirlanda G., 2011, MNRAS, in press (G11)
- Landt H., Padovani P. & Giommi P., 2002, MNRAS, 336, 945
- Landt H., Padovani P., Giommi P. Perlman E.S., 2004, MNRAS, 351, 83
- León-Tavares J., Valtaoja E., Chavushyan V.H. et al., 2011, MNRAS, 411, 1127
- Mahadevan R., 1997, ApJ, 447, 585
- Marcha M.J.M., Browne I.W.A., Impey C.D. & Smith P.S., 1996, MNRAS, 281, 425
- Mattox J.R., Bertsch D.L., Chiang J., et al., 1996, ApJ, 461, 396
- Narayan R., Garcia M.R. & McClintock J.E., 1997, ApJ, 478, L79
- Narayan R. & Yi I., 1995, ApJ, 452, 710
- Padovani P., 1992, A&A, 256, 399
- Padovani P. & Giommi P., 1995, ApJ, 444, 567
- Plotkin R.M., Anderson S.F., Hall P.B. et al., 2008, AJ, 135, 2453

- Plotkin R.M., Anderson S.F., Brandt W.N. et al., 2010, AJ, 139, 390  
 Plotkin R.M., Markoff S., Trager S.C. & Anderson S.F., 2011, MNRAS, 413, 805 (P11)  
 Scarpa R., Falomo R., 1997, A&A, 325, 109  
 Shakura N.I. & Sunyaev R.A., 1973 A&A, 24, 337  
 Sharma P., Quataert E., Hammet G.H. & Stone J.M., 2007, ApJ, 667, 714  
 Shen Y., Richards G.T., Strauss M.A. et al., 2011, ApJS, 194, 45 (S11)  
 Smith M.G., Carswell R.F., Whelan J.A.J. et al., 1981, MNRAS 195, 437  
 Tavecchio F., Ghisellini G., Ghirlanda G., Foschini L. & Maraschi L., 2010, MNRAS, 401, 1570  
 Urry C.M. & Padovani P., 1995, PASP, 107, 803  
 White R.L., Becker R.H., Helfand D.J., & Gregg M.D., 1997, ApJ, 475, 479  
 York D.G., Adelman J., Anderson J.E. et al., 2000, AJ, 120, 1579

## 7 APPENDIX

### 7.1 Spectral energy distribution

We have characterized the Spectral Energy Distribution (SED) of the six sources for which we have both the spectroscopic optical data and the detection by *Fermi*.

To this aim we have collected the data from the NASA Extragalactic Database (NED) and including the LBAS and 1LAC *Fermi*/LAT data (Abdo et al. 2010a; 2010b).

### 7.2 The model

To model the SED we have used the leptonic, one-zone synchrotron and inverse Compton model, fully discussed in Ghisellini & Tavecchio (2009).

In brief, we assume that in a spherical region of radius  $R$ , located at a distance  $R_{\text{diss}}$  from the central black hole, relativistic electrons are injected at a rate  $Q(\gamma)$  [ $\text{cm}^{-3} \text{s}^{-1}$ ] for a finite time equal to the light crossing time  $R/c$ . For the shape of  $Q(\gamma)$  we adopt a smoothly broken power law, with a break at  $\gamma_b$ :

$$Q(\gamma) = Q_0 \frac{(\gamma/\gamma_b)^{-s_1}}{1 + (\gamma/\gamma_b)^{-s_1+s_2}} \quad (4)$$

The emitting region is moving with a velocity  $\beta c$  corresponding to a bulk Lorentz factor  $\Gamma$ . We observe the source at the viewing angle  $\theta_v$  and the Doppler factor is  $\delta = 1/[\Gamma(1 - \beta \cos \theta_v)]$ . The magnetic field  $B$  is tangled and uniform throughout the emitting region. We take into account several sources of radiation externally to the jet: i) the broad line photons, assumed to re-emit 10% of the accretion luminosity from a shell-like distribution of clouds located at a distance  $R_{\text{BLR}} = 10^{17} L_{\text{d,45}}^{1/2} \text{ cm}$ ; ii) the IR emission from a dusty torus, located at a distance  $R_{\text{IR}} = 2.5 \times 10^{18} L_{\text{d,45}}^{1/2} \text{ cm}$ ; iii) the direct emission from the accretion disc, including its X-ray corona; iv) the starlight contribution from the inner region of the host galaxy; v) the cosmic background radiation. All these contributions are evaluated in the blob comoving frame, where we calculate the corresponding inverse Compton radiation from all these contributions, and then transform into the observer frame. The latter two contributions are negligible for our sources.

We calculate the energy distribution  $N(\gamma)$  [ $\text{cm}^{-3}$ ] of the emitting particles at the particular time  $R/c$ , when the injection process ends. Our numerical code solves the continuity equation which includes injection, radiative cooling and  $e^\pm$  pair production and reprocessing. Our is not a time dependent code: we give a “snapshot” of the predicted SED at the time  $R/c$ , when the particle distribution  $N(\gamma)$  and consequently the produced flux are at their maximum.

To calculate the flux produced by the accretion disc, we adopt a standard Shakura & Sunyaev (1973) disc (see Ghisellini & Tavecchio 2009).

The resulting SEDs and models are shown in Fig. 6, Fig. 7 and Fig. 8, and the model parameters are reported in Tab. 6 and Tab. 7.

### 7.3 Specific sources

We here discuss briefly a few objects for which we do have both the information on the BLR and the  $\gamma$ -ray luminosity. These sources lie close to the “intermediate zone” between BL Lacs and FSRQs. We have constructed their SED and modeled it through a simple one-zone leptonic model, as described in Section 7.2, in order to classify them. To this aim we adopt the same SED-based classification scheme discussed in G11 and originally introduced by

Padovani & Giommi (1995). In brief, we can classify the object as a FSRQ if the  $\gamma$ -ray luminosity is dominating the electromagnetic output and if the X-ray spectrum is flat (X-ray energy spectral index  $\alpha_x < 1$ ); it is a Low frequency peaked BL Lac (LBL) if the  $\gamma$ -ray luminosity is comparable to the synchrotron one and if  $\alpha_x < 1$ , and high frequency peaked BL Lac (HBL) if the  $\gamma$ -ray luminosity is comparable or less than the synchrotron one and  $\alpha_x > 1$ . Fig. 6, Fig. 7 and Fig. 8 show the SED of these sources. We here summarize our finding.

**0937+5008** — This source is included in the S11 catalog and it is detected by *Fermi*. Looking at the SED it can be clearly classified as a FSRQ, as suggested also from the evident broad H $\alpha$  and H $\beta$  lines visible in the SDSS spectrum. From the SED modeling, a synchrotron contamination of the optical continuum is visible. Therefore, the automatic virial black hole mass estimate performed by S11 can be imprecise. Hence, we chose to assign to its black hole an average mass value  $M = 5 \times 10^8 M_\odot$ .

**1040+24** — This is a DR6 *Fermi* detected source, hence the black hole mass is not measured. We can assume an average value of  $M = 5 \times 10^8 M_\odot$ . In the SDSS spectrum, a broad MgII line is clearly visible. From the SED modeling, this source can be classified as a LBL. This means that the thermal continuum can be highly contaminated by the synchrotron emissions, although some broad emission lines clearly emerge. Moreover, the disc seems to be only partially covered, and the synchrotron component looks really variable. This could result in a variable line EW.

**1055+01** — This source belongs to the DR6+1LAC sample, hence the mass is not measured and we assume the average value  $M = 5 \times 10^8 M_\odot$ . As in the case of 1040+24, a broad MgII line is visible, but it is narrower than the usual broad emission line width ( $\text{FWHM} \simeq 2500 \text{ km s}^{-1}$ ). This might suggest a small black hole mass, or maybe the line is partially covered by the continuum and hence the measure is uncertain. The SED, indeed, shows that the accretion disc contribution is mostly covered by the synchrotron emission. Overall, we can classify this source as a FSRQ, even if the disc emission is dominated by the synchrotron radiation.

**1106+023** — It is a DR6 source detected by *Fermi*. In this case we can estimate its mass with the Chiaberge & Marconi (2011) relation. In fact the FWHM of its broad H $\beta$  line is reported in the DR6 catalog. The mass estimate that we obtain is very small ( $M = 4 \times 10^7 M_\odot$ ). From the SED, we can see that the disc emerges from the synchrotron component, hence the emission lines can be seen clearly. From the SED we can classify this source as a LBL.

**1117+2014** — This source is present in the S11 catalog, hence it is supposed to be a quasar. However, in the SDSS spectrum, the H $\beta$  line is really faint. Indeed, from the SED modeling, we can classify this source as an HBL. The SED shows clearly that the synchrotron component largely dominates the disc emission, hence the automatic mass estimate performed by S11 ( $M = 4 \times 10^8 M_\odot$ ) is not accurate. We then assume for this source a value of the black hole of equal to the average value.

**1509+022** — This is a source included in the S11 catalog. Looking at the SED, we can classify it as a FSRQ. However, also in this case the continuum appears contaminated by the synchrotron component. Moreover, the S11 results about this source are quite unclear. The equivalent widths reported in S11 ( $\text{EW} \sim 25 - 27 \text{ \AA}$ ), do not seem to be recognizable in the spectrum (the lines are hardly visible). Therefore, we think that the S11 black hole mass estimate

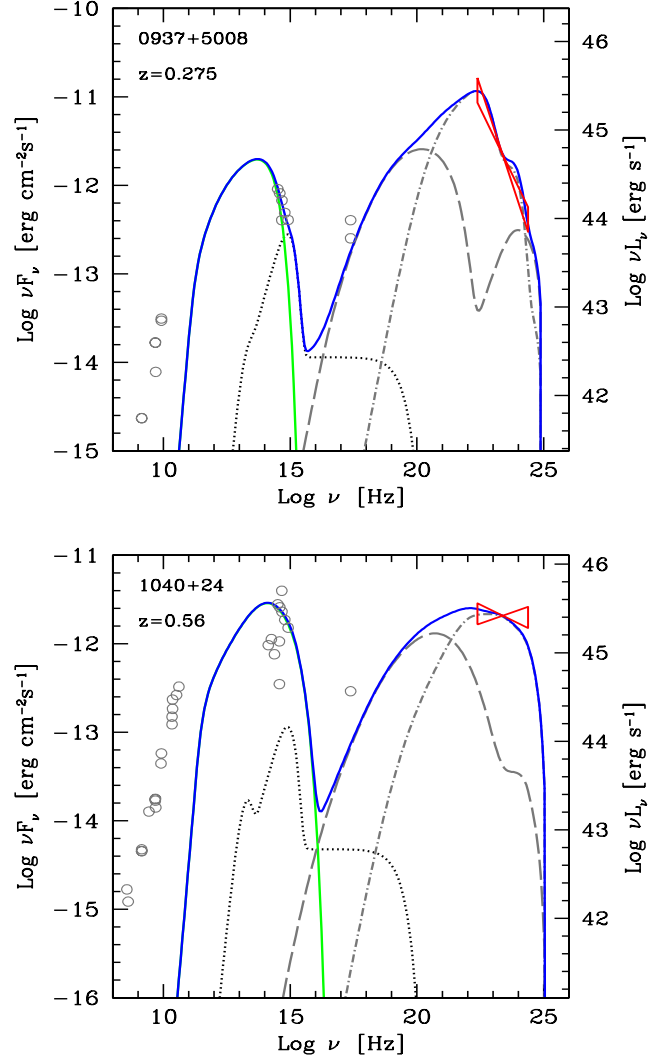


**Figure 6.** SED of 0937+5508 and 1040+24 and the fitting model. The dotted line corresponds to emission from the accretion disc, the IR torus (if present) and the X-ray corona, the thin (green) solid line is the synchrotron component, the long dashed line the SSC emission, the dot-dashed line the EC contribution. The thick (blue) solid line is the sum.

can be considered imprecise, and we replace it with the average value  $M = 5 \times 10^8 M_\odot$ .

Name [1]	$z$ [2]	$R_{\text{diss}}$ [3]	$M$ [4]	$R_{\text{BLR}}$ [5]	$P'_i$ [6]	$L_d$ [7]	$B$ [8]	$\Gamma$ [9]	$\theta_v$ [10]	$\gamma_b$ [11]	$\gamma_{\text{max}}$ [12]	$s_1$ [13]	$s_2$ [14]
0937+5008	0.275	90 (600)	5e8*	34.6	2e-3	0.12 (1.6e-3)	0.14	14	3	400	5e3	0	2.5
1040+23	0.56	97.5 (650)	5e8*	51.2	1.5e-3	0.26 (3.5e-3)	0.67	13	3	100	9e3	0	2
1055+01	0.888	105 (700)	5e8*	98.7	0.02	0.98 (0.013)	3.1	11	3.7	400	9e3	1	2.5
1106+023	0.157	43.2 (3.6e3)	4e7	21.9	3e-3	0.048 (8e-3)	0.22	13	3	6e3	6e3	2	2
1117+2014	0.138	105 (700)	5e8*	13.7	5.e-5	0.019 (2.5e-4)	0.7	15	2	3e4	1.5e5	0.5	3
1509+022	0.2194	120 (800)	5e8*	34.6	0.022	0.12 (1.6e-3)	0.13	11	6	100	2e4	0	2.3

**Table 6.** List of parameters used to construct the theoretical SED. Col. [1]: name; Col. [2]: redshift; Col. [3]: dissipation radius in units of  $10^{15}$  cm and (in parenthesis) in units of Schwarzschild radii; Col. [4]: black hole mass in solar masses, the asterisk means that the mass is assumed; Col. [5]: size of the BLR in units of  $10^{15}$  cm; Col. [6]: power injected in the blob calculated in the comoving frame, in units of  $10^{45}$  erg  $\text{s}^{-1}$ ; Col. [7]: accretion disc luminosity in units of  $10^{45}$  erg  $\text{s}^{-1}$  and (in parenthesis) in units of  $L_{\text{Edd}}$ ; Col. [8]: magnetic field in Gauss; Col. [9]: bulk Lorentz factor at  $R_{\text{diss}}$ ; Col. [10]: viewing angle  $\theta_v$  in degrees; Col. [11] and [12]: break and maximum random Lorentz factors of the injected electrons; Col. [13] and [14]: slopes of the injected electron distribution  $[Q(\gamma)]$  below and above  $\gamma_b$ ; The total X-ray corona luminosity is assumed to be in the range 10–30 per cent of  $L_d$ . Its spectral shape is assumed to be always  $\propto \nu^{-1} \exp(-h\nu/150 \text{ keV})$ .

Name	$\log P_r$	$\log P_B$	$\log P_e$	$\log P_p$
0937+5008	43.49	42.06	44.47	45.05
1040+23	43.89	43.43	44.08	44.99
1055+01	45.31	44.69	44.68	46.67
1106+023	42.87	41.76	44.58	46.94
1117+2014	42.98	43.66	42.46	42.27
1509+022	44.42	42.04	45.04	46.03

**Table 7.** Logarithm of the jet power in the form of radiation, Poynting flux, bulk motion of electrons and protons (assuming one proton per emitting electron). Powers are in erg  $\text{s}^{-1}$ .

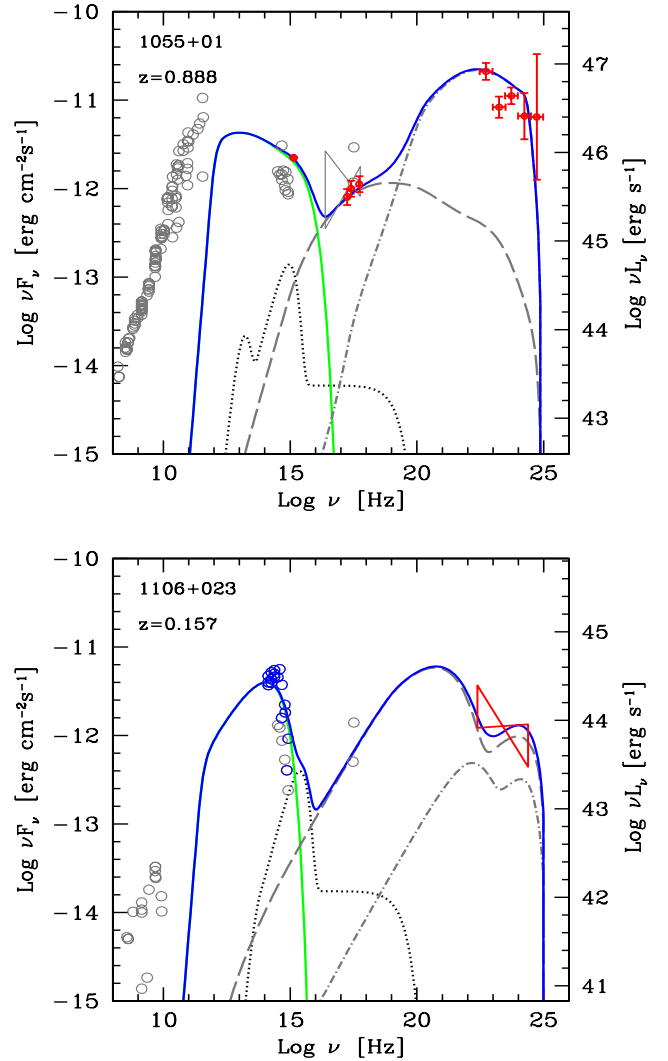


**Figure 7.** SED of 1055+01 and 1106+023. Lines as in Fig. 6.



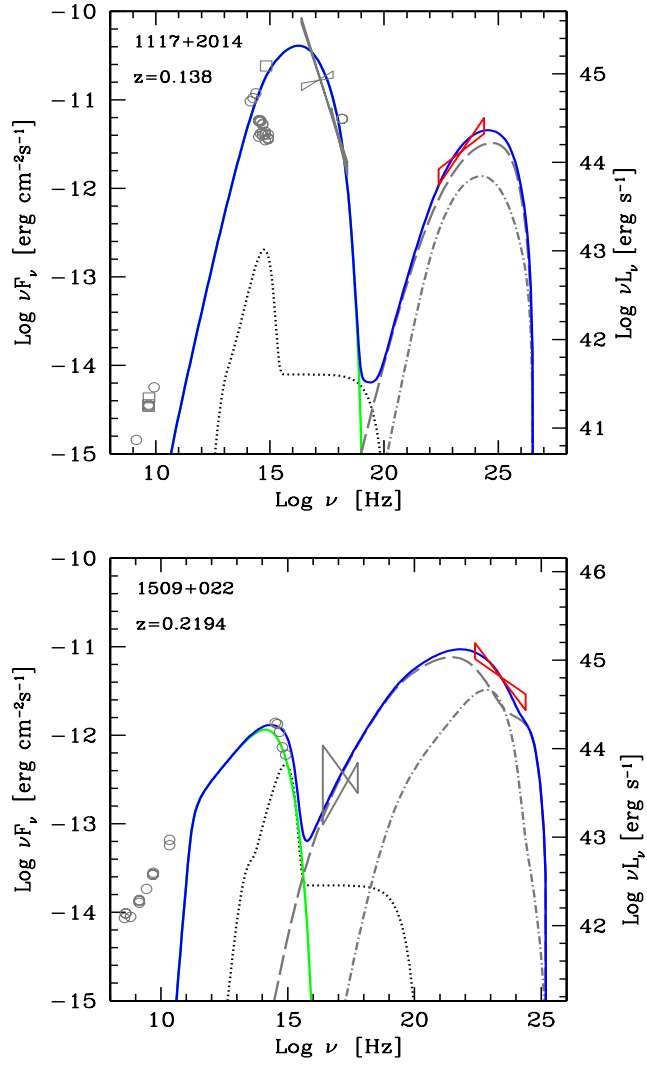


**Figure 8.** SED of 1117+2014 and 1509+022. Lines as in Fig. 6.